Check for updates

Simple and convenient mapping of molecular dynamics mechanical property predictions of bisphenol-F epoxy for strain rate, temperature, and degree of cure†

Sagar U. Patil, [ID] [a] Aaron S. Krieg, [ID] [a] Leif K. Odegard, [a] Upendra Yadav, [a] Julia A. King, [a] Marianna Maiaru [b] and Gregory M. Odegard [ID] *[a]

It is well-known that all-atom molecular dynamics (MD) predictions of mechanical properties of thermoset resins suffer from multiple accuracy issues associated with their viscoelastic nature. The nanosecond simulation times of MD simulations do not allow for the direct simulation of the molecular conformational relaxations that occur under laboratory time scales. This adversely affects the prediction of mechanical properties at realistic strain rates, intermediate degrees of cure, and elevated temperatures. While some recent studies have utilized a time-temperature superposition approach to relate MD predictions to expected laboratory observations, such an approach becomes prohibitively difficult when simulating thermosets with a combination of strain rates, intermediate degrees of cure, and temperatures. In this study, a phenomenological approach is developed to map the predictions of Young's modulus and Poisson's ratio for a DGEBF/DETDA epoxy system to the corresponding laboratory-based properties for intermediate degrees of cure and temperatures above and below the glass transition temperature. The approach uses characterization data from dynamical mechanical analysis temperature sweep experiments. The mathematical formulation and experimental characterization of the mapping is described, and the resulting mapping of computationally-predicted to experimentally-observed elastic properties for various degrees of cure and temperatures are demonstrated and validated. This mapping is particularly important to mitigate the strain-rate effect associated with MD predictions, as well as to accurately predict mechanical properties at elevated temperatures and intermediate degrees of cure to facilitate accurate and efficient composite material process modeling.

1. Introduction

Thermosetting polymer composites are extensively used in the aerospace industry because of their relatively low mass density and unique combination of mechanical, thermal, and electrical properties. Computationally-driven design of new generations of thermoset composites for improved performance requires multiscale modeling techniques that are powerful and reliable. Such multiscale modeling must be able to incorporate molecular-scale structure for the prediction of structural-level properties. In particular, molecular dynamics (MD) methods

need to be developed that can efficiently predict accurate properties of thermoset neat resins as input into higher-length scale modeling techniques.

Thermoset neat resins consist of a complex network of covalently-linked molecular segments. Generally, for a given state of external conditions (*e.g.* temperature, mechanical deformation) these segments change their conformation to reach a state of lower energy (relaxation), which ultimately manifests itself as the phenomena known as physical aging and viscoelasticity.[1] These relaxation processes can occur over a wide range of time periods spanning nanoseconds to years, but a significant portion of them occur over timescales associated with composite laminate processing and laboratory mechanical testing. Although all-atom MD simulations have been used over the last several decades to predict molecular structure and nano-scale properties of thermoset resins,[2–16] these simulations can only capture the thermoset network response over a nanosecond time scale, creating a significant discrepancy

[a] *Michigan Technological University, Houghton, MI-49931, USA.*
  E-mail: gmodegar@mtu.edu
[b] *University of Massachusetts, Lowell, MA-01854, USA*

between simulated and laboratory timescales. Although coarse-grain simulation techniques[17–21] can be used to somewhat avert the time scale limitation over a broad range of frequencies, atomistic details often play a more significant role at higher frequencies.

Because of the timescale discrepancy between the conformational response on laboratory and MD-based timescales, all-atom MD predictions cannot precisely capture the relaxation processes that occur over time increments above nanoseconds. This shortcoming manifests itself in three major ways. First, MD predictions of fully crosslinked thermosets slightly overestimate the room-temperature elastic properties and yield strength.[7,8,15] This is commonly referred to as the "strain rate effect". Second, MD predictions of mechanical properties above the glass transition temperature (T_g) significantly overestimate experimental observations. Whereas the measurements indicate a multiple order-of-magnitude drop in elastic modulus relative to room temperature,[22] simulations predict only about a 50% drop.[22] Third, MD predictions of partially-crosslinked epoxies indicate a steady increase in elastic modulus over the entire range of degrees of cure,[15] whereas experiments show a negligible modulus for all levels of crosslinking below the nearly fully-crosslinked state.[15,22] These three manifestations of the viscous response have the same origin. During simulated mechanical deformations, conformational relaxation processes are not given sufficient time to occur, and thus the associated energy relaxation does not occur, resulting in a stiffer apparent structural response of the network. That is, quantities such as shear modulus and Young's modulus are overpredicted relative to their experimentally-measured values. Decreases in the degree of cure and increases in temperature exaggerate this effect, as they increase the viscous response of the material.

Multiple methods have been proposed to account for the predicted modulus discrepancy in fully crosslinked systems at room temperature.[23–27] However, a convenient and comprehensive approach that accounts for the viscous response of thermosets in MD predictions of mechanical properties for various levels of strain rates, temperatures, and degrees of cure has not been established. Such a method should have three minimum requirements. First, the method should involve minimal MD simulations. One approach to capturing the viscoelastic effect of polymers in MD predictions is to use a time-temperature superposition principle.[10,25–29] Approaches like this require significant computational resources to fully characterize each polymer system considered, especially for multiple degrees of cure. In a materials engineering environment where computational material design and process optimization need to be performed as efficiently as possible, a full MD-based characterization of the time-temperature superposition is not feasible and does not directly address the dependency of degree of cure on the viscous response. Also, it is important to note that the time-temperature superposition principle can sometimes fail for some polymer systems[30,31] and is thus not a comprehensive solution.

Second, the method should require minimal experimental input (although no experimental input is ultimately desired).

Bulk-level characterization of the material response as a function of strain rate, temperature, and degree of cure can be performed by experiment. However, such an approach is prohibitively time-consuming and expensive for most composite material development applications and does not capture molecular-scale events and the bulk behavior at relatively high strain rates. Third, the method should directly address all three of the above-mentioned manifestations of the viscous response of thermosets.

In this work, a comprehensive approach satisfying all the above-mentioned criteria to establish a phenomenological viscous response mapping factor is proposed for correlating elastic properties predicted with all-atom MD simulations to those expected at laboratory-scale timeframes. In addition, experimental characterization of thermal and mechanical properties of epoxy for different mixing ratios to efficiently emulate a range of degrees of cure[32,33] is performed to inform the mapping procedure. It is important to emphasize that this approach is phenomenological and is designed to be parameterized by a convenient set of experiments to quickly map MD predictions for rapid computationally-driven thermoset material design. It is not intended to be a comprehensive viscoelastic characterization of a resin *via* classical viscoelastic constitutive modeling.[34,35] This article is organized as follows: first the methodology to establish the viscous response mapping is introduced, followed by a description of the experimental methods used to characterize the mapping. The parameterization and optimization of the mapping is then described, and results of the modeling with the mapping technique follow. The results show that the proposed approach effectively provides an accurate mapping for MD predicted Young's moduli of thermosets to capture the effects of strain rate, temperature, and degree of cure.

The significance of this work is that, for the first time, a relatively simple and efficient modeling approach has been developed that maps elastic properties predicted from MD simulations (which are naturally over-predictive because of the simulated high strain rates) to those that would be expected if MD could be run at times scales associated with experimental measurements of elastic properties (seconds, minutes, hours, *etc.*). The proposed mapping approach does not require rigorous time-temperature superposition relationships (which are difficult and time-consuming to establish), and thus provides efficient corrections to MD-predicted elastic properties that can be immediately utilized in multi-scale, computationally-driven material and structural design.

2. Viscous correction

Using an approach inspired by the Buckingham π theorem,[36] the viscous response can be expressed in terms of a minimal set of dimensionless parameters. It is first assumed that a laboratory-scale mechanical property (specifically, the Young's modulus in this case) can be related to its MD-predicted value by

$$\frac{E}{E_{MD}} = f(\dot{\varepsilon}, \phi, T) \tag{1}$$

where $\dot{\varepsilon}$ is the strain rate, ϕ is the degree of cure, T is the temperature, E is the laboratory-scale Young's modulus, and E_{MD} is the all-atom MD-predicted Young's modulus in the fully crosslinked system at room temperature and MD-scale strain rates. The function f is thus limited to the range of $0 \leq f \leq 1$. The degree of cure is a dimensionless parameter valued between 0 (completely uncured) and 1 (fully cured). It is important at this point to discuss the assumptions associated with eqn (1). It is assumed that as strain rates decrease towards laboratory-based strain rates and the degree of cure approaches the maximum value of 1, the MD-predicted modulus approaches the value that is experimentally-measured at the corresponding temperature. If MD simulations could be run long enough (or fast enough), then E_{MD} would naturally approach E, however, currently this is not feasible. Of course, for very long simulation times, E_{MD} will only approach E if the simulation also accurately captures topological features such as porosity, chain/network morphology, *etc.* Additionally, EMD can only approach E if the molecular-level interactions are accurately captured with an appropriate force field. For example, the Interface Force Field (IFF)[37] has been shown to accurately capture bulk physical, mechanical, and thermal properties of thermosets[7,38] and thermoplastics.[39]

Dimensionless parameters can now be introduced such that this formulation is independent of units and contains functions with direct proportionality with the dependent variable (modulus ratio). Specifically, the following dimensionless variables are defined:

$$\alpha \equiv \frac{\dot{\varepsilon}}{\dot{\varepsilon}_{MD}}, \quad \tau \equiv 1 - \frac{T}{T_r}$$

where $\dot{\varepsilon}_{MD}$ is the strain rate associated with MD time scales (for example, $1 \times 10^8 \text{ s}^{-1}$); T_r is the reference temperature, which should be the highest temperature for which experimental Young's modulus data is available, and herein will be assigned as the processing temperature of the thermoset resin; and T and T_r are expressed in degrees Kelvin. Thus, α and τ are dimensionless scalars that are valued between 0 and 1. Eqn (1) can be re-written in terms of the dimensionless parameters

$$\frac{E}{E_{MD}} = f(\alpha, \phi, \tau) \tag{2}$$

For simplicity, eqn (2) can be further specified using a separation-of-variables approach, where $f(\alpha, \phi, \tau)$ is approximated as a product of lower-dimension functions of the independent variables. If we choose the lower-dimension functions to represent the viscous response to strain rate (f_α), degree of cure (f_ϕ), and temperature (f_τ), then such a function could be represented as

$$\frac{E}{E_{MD}} = f_\alpha(\alpha) f_\phi(\phi) f_\tau(\tau, \phi) \tag{3}$$

where each of the functions f_α, f_ϕ, and f_τ are directly proportional to their corresponding independent variables, and are valued between 0 and 1. It is important to note that the

separation of variables approach, which is famously used for the solution of the wave function in quantum mechanics[40] is not rigorous and is only chosen out of necessity and intuition. Note that the function associated with temperature, f_τ, is a function of both ϕ and τ because the temperature response (glass transition temperature) of a thermoset is dependent both on temperature and degree of cure. Although the temperature response could also be a function of strain rate (for example, in a mechanical test that varies the temperature and deformation rate), it is assumed that the strain rate is appropriately captured by the f_α function. The functional forms and parameters associated with functions in eqn (3) are determined using data from the literature and experiments, as described below. It is also important to note that the mechanical response of polymers is often characterized in the frequency domain instead of the strain rate domain. It is assumed here that the frequency response is captured with the strain rate response function, f_α. Coupling between the degree of cure and the frequency response is assumed, out of simplicity and ease of characterization, to be captured by the product of f_α and f_ϕ. Although this may not be rigorously and physically accurate, it is assumed to suffice for the purposes of this study.

There is one other important point to discuss in terms of eqn (3). The intent of eqn (3) is not to reproduce the rigorous mapping associated with the time-temperature superposition principle. If the full time-temperature superposition principle was comprehensively known *a priori* for thermoset systems for which it is valid, then the approach discussed herein would not be necessary. For polymer systems in which the time-temperature superposition principle fails, there is no clear alternative predictive approach. Either way, eqn (3) provides an efficient means to map raw MD-predicted properties to the corresponding properties that would be expected at laboratory time scales and temperatures. This is important in computationally-driven materials discovery, developing digital twins, and integrated computational materials engineering; in which material discovery and development needs to be performed efficiently and within the context of higher-length scale modeling. It is important to note that machine learning can be utilized to characterize eqn (2) directly. However, for such analyses, abundant well-curated data is necessary, as previously shown for other computational-based composites research.[41] For this study, eqn (3) was utilized because sufficient data was not available for a rigorous machine-learning parameterization.

3. Material

The chosen material for the parameterization of eqn (3) is an epoxy system consisting of a diglycidyl ether bisphenol F (DGEBF) epoxide monomer with a diethyltoluenediamine (DETDA) curing agent, as shown in Fig. 1. These materials are commonly marketed as EPON 862 and EPIKURE W, respectively. This system was chosen because it is highly benchmarked and represents a baseline high-performance thermoset.
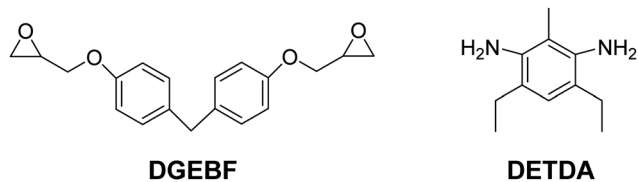
Fig. 1 DGEBF/DETDA epoxy system molecular structure.

4. Experimental details

This section describes the details of the experiments performed to parameterize eqn (3). The experiments were performed on the DGEBF/DETDA epoxy system with a range of mixing ratios as proxies to various degrees of cure.[32,33] The use of these proxies was necessary because of the high level of difficulty of testing thermal properties of thermoset systems as a function of degree of cure. Although it is acknowledged that the use of off-stoichiometry systems is not a direct substitute for fully stoichiometric systems with intermediate degrees of cure, the proxies provide a reasonable substitute that is relatively easy to fabricate and test. It is also important to note that the parameterization of eqn (3) is based purely on experimental data, not on MD-generated data.

Epoxy samples were manufactured using a compression molding method. A total of two speedmixer cups were each charged with 50 g of DGEBF epoxy resin and an appropriate amount of DETDA curing agent to achieve systems with seven different mixing ratios of resin and hardener (Table 1). The mixing ratio is defined as the ratio of the mass of the actual DETDA hardener with respect to the mass of the DETDA hardener in the fully stoichiometric mixture. Speedmixer cups were mixed in a FlackTek Speedmixer (DAC 150.1 FVZ) at 2000 rpm for 5 minutes at 25 °C and then heated to 90 °C in a vacuum oven. The speedmixer cups were degassed in the vacuum oven at 90 °C for 30 minutes at 0.101 MPa vacuum pressure. The resin system was cast into a tooling assembly and compression molded at 121 °C for 2 hours and then ramped to 177 °C and held for 2 hours. The compression molder was cooled using air and water until the system was cooled to 150 °C and then was switched to water cooling only to continue cooling the system to 25 °C before removing the plate. The tooling assembly produced 152.4 × 152.4 mm plates with 3.2 mm thickness.

Dynamic mechanical analysis (DMA) was used to determine the thermo-mechanical response of the epoxy as a function of temperature and degree of cure. The testing was performed for all mixing ratios shown in Table 1 to approximate the corresponding degrees of cure. The DMA specimens were cut from fabricated plates using a vertical bandsaw. Three specimens were tested for each mixing ratio. The specimens were 38.1 mm long, 12.7 mm wide, and 3.2 mm thick and the tests were performed using a TA Instruments Q800 DMA in single cantilever test mode with a constant frequency of 1 Hz, an amplitude of 25 μm, and a ramp rate of 3 °C min^{-1}. For this study, constant frequency of 1 Hz was utilized, as varying frequencies have shown no significant effect on the storage moduli measured using DMA tests of high-performance resins.[42] The storage modulus, loss modulus, and tan delta values were continuously monitored during the temperature sweep. The storage modulus for all of the mixing ratios is shown in Fig. 2a for the whole range of temperatures. From this data, it is evident that the transition from glassy to rubbery states occurs at decreasing temperatures with decreasing levels of DETDA (thus degree of cure).

Fig. 2b shows the same data as Fig. 2a, but with the vertical axis scale focused on small values of storage modulus. The purpose of this graph is to show the details of the storage modulus curves above T_g for each mixing ratio. Even the post-T_g curves in Fig. 2a appear to drop to zero, Fig. 2b shows that they are not zero-valued above T_g, they are 2–3 orders of magnitude smaller than their respective values below T_g.

Fig. 2c shows the storage modulus as a function of mixing ratio at room temperature. It can be seen from the plot that the storage modulus gradually increases from the fully stoichiometric level with decreasing mixing ratios until 65%. This is likely because of increasing levels of mass density of the proxy systems as DETDA monomers are removed. Fully stoichiometric systems with intermediate degrees of cure are not expected to exhibit this behavior, and this is the primary disadvantage of using proxy systems. However, as described below, this behavior did not affect the viscous response parameterization, and the advantages of using proxy systems for the purposes of this study far outweigh this disadvantage. In Fig. 2c, it is also observed that as the mixing ratio decreases below 65%, the storage modulus drastically decreases as the sparse network can no longer sustain significant mechanical loads.

The T_g was determined using three different metrics: storage modulus, loss modulus, and tan delta. To determine the T_g using the storage modulus, the onset of the decline in storage modulus was located by finding the intersection between the baseline and the tangent at the point of the highest slope. The T_g values for the loss modulus and tan delta metrics were determined from the peak of the loss modulus and tan delta curves, respectively. Fig. 2d shows the T_g values as a function of mixing ratio using all three metrics. It is clear that the T_g trends from the three metrics are very similar with mixing ratio, with only a difference in the magnitude. From Fig. 2(c) and (d), no significant deviation in the measured storage modulus and T_g was observed between the three specimens. For storage modulus and T_g (all three metrics) the standard deviations are within 3% and 1% respectively.

Table 1 Mixing ratios for DGEBF/DETDA systems

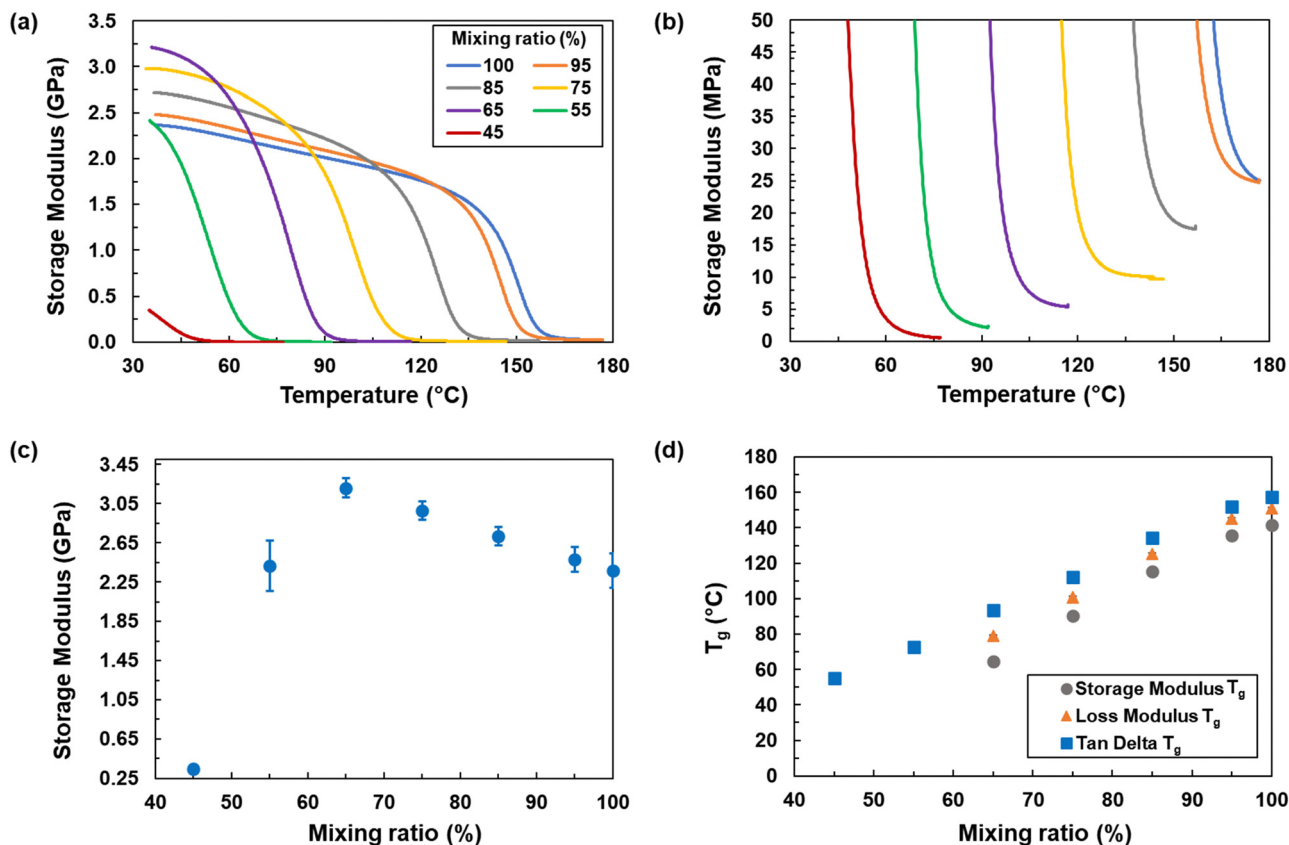| Mixing ratio (%)	DGEBF (g)	DETDA (g)
100	100	26.4
95	100	25.1
85	100	22.4
75	100	19.8
65	100	17.2
55	100	14.5
45	100	11.9

Fig. 2 (a) Representative curves of storage modulus *vs.* temperature, (b) representative curves of storage modulus *vs.* temperature near the *x*-axis, (c) storage modulus *vs.* mixing ratio (*n* = 3) at room temperature, (d) T_g *vs.* mixing ratio (*n* = 3), where the standard deviations are smaller than the symbols.

5. Viscous mapping parameterization

The specific forms of functions in eqn (3) and the corresponding phenomenological parameters for the DGEBF/DETDA system were determined as described in this section. First, the specific forms of the functions and the initial guesses of the parameters are outlined, followed by a description of the parameter optimization using the Newton–Raphson[43] iterative numerical technique.

5.1 Functional forms, parameters, and initial guesses

It has been demonstrated[6,7,9] that the DGEBF/DETDA system shows a logarithmic dependance of elastic modulus and yield strength on strain rate over a range of strain rates spanning experimental timescales (10^{-5} s^{-1}) to those associated with MD simulations (10^{9} s^{-1}) for fully crosslinked systems at room temperature. Therefore, $f(\alpha)$ can be expressed as

$$f_\alpha(\alpha) = \alpha_a \ln(\alpha) + \alpha_b \qquad (4)$$

where α_a and α_b are phenomenological parameters. These parameters can be determined by fitting experimental data of the Young's modulus normalized by the modulus predicted by MD (such that $0 \leq f_\alpha \leq 1$) as a function of α. Fig. 3a shows such a fit using several experimental data points from the literature,[38,44–46] with dimensionless least-square fitting parameters α_a = 0.0147 and α_b = 1.0849. Eqn (4) is purely empirical

and is not derived from first principles. There is no physical significance to the mathematical form, as it is a curve fit to the experimental data that is extrapolated to the higher decades of strain rate. The limits of eqn (4) are simply the strain rate decades that it is intended for, namely 10^{-5} s^{-1} to 10^{9} s^{-1}. The ESI,† provides a brief analysis of the effect of the scatter on the predicted Young's modulus. It is important to emphasize that the form of eqn (4) is based only on the DGEBF/DETDA system data published previously,[6–8] even though ref. 7 and 8 indicate that the relationship can be used to model the strain rate effect of other thermoset systems. In general, the form of eqn (4) can change for different thermoset systems, which can be the subject of future studies on a wider range of thermosetting chemistries.

As shown in Fig. 2c, the storage modulus exhibits a sigmoid-type response as a function of degree of cure. Thus, a logical choice for the $f_\phi(\phi)$ functional form is a Fermi–Dirac function,[47] whose value ranges between 0 and 1 and describes a continuous, yet step-like change from 0 to 1 centered at ϕ_0 with a step change intensity described by ϕ_σ:

$$f_\phi(\phi) = 1 - \left[1 + e^{\left(\frac{\phi-\phi_0}{\phi_\sigma}\right)}\right]^{-1} \qquad (5)$$

Using the data shown in Fig. 2c, values of ϕ_0 and ϕ_σ were determined by focusing the center of the sigmoid on the
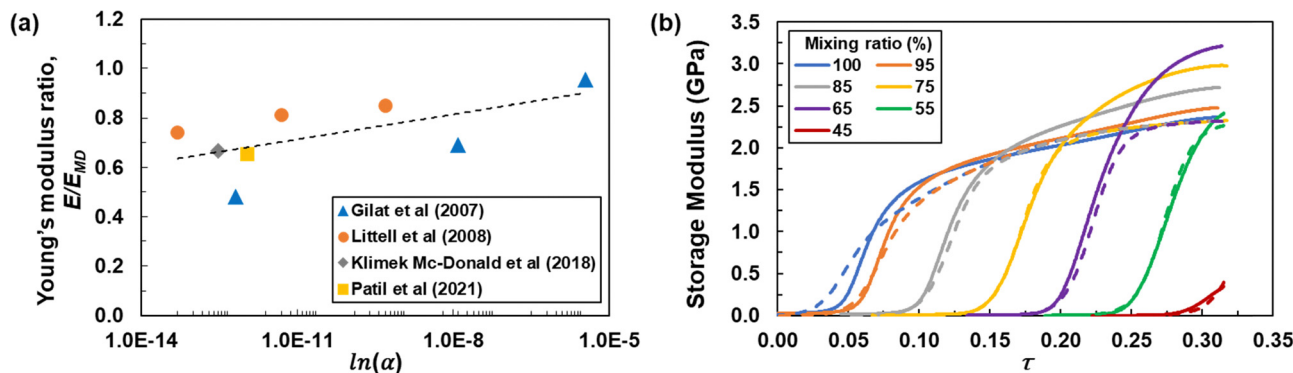
Fig. 3 (a) Normalized Young's modulus of DGEBF/DETDA epoxy as a function of applied normalized strain rate determined experimentally, (b) plot of storage modulus *vs.* τ. Solid lines are data from the DMA experiments, and dashed lines are from eqn (3)–(8) with the optimized parameters from Table 2.

drop in modulus between degrees of cure of 45 and 55%. The corresponding dimensionless values are $\phi_0 = 0.45$ and $\phi_\sigma = 0.02$.

From the data shown in Fig. 2a, it is clear that the modulus exhibits a sigmoid-type response with respect to temperature. Furthermore, it is evident that this temperature response is dependent on the degree of cure of the thermoset. Therefore, a functional form of $f(\tau,\phi)$ that captures this dependance is

$$f_\tau(\tau, \phi) = \left\{ 1 - \left[1 + e^{\left(\frac{\tau - \tau_0(\phi)}{\tau_\sigma}\right)} \right]^{-1} \right\} \tau_*(\tau) \qquad (6)$$

where $\tau_0(\phi)$ corresponds to the center of the sigmoidal-type response associated with the glass transition, which is dependent on ϕ; τ_σ describes the step change intensity of the transition; and $\tau^*(\tau)$ describes the change in the mechanical properties with temperature under the T_g. The value of τ_0 can be described with

$$\tau_0(\phi) = \tau_0^a \phi + \tau_0^b \qquad (7)$$

where τ_0^a and τ_0^b are dimensionless phenomenological parameters. The value of τ_* is described by

$$\tau_*(\tau) = 1 - \left[1 + e^{\left(\frac{\tau - \tau_*^a}{\tau_*^b}\right)} \right]^{-1} \qquad (8)$$

where τ_*^a and t_*^b are dimensionless phenomenological parameters. The parameters in eqn (6)–(8) were determined using the DMA data shown in Fig. 2a. The same data is plotted in Fig. 3b *versus* τ for all mixing ratios. The parameters τ_0^a and τ_0^b were determined by locating the sigmoid centers of the data in Fig. 3b for the different degrees of cure and fitting those values to the linear function shown in eqn (7). The best-fit values were $\tau_0^a = -0.4712$ and $\tau_0^b = 0.5268$. It is important to note that eqn (6) predicts values that quickly approach zero as the temperature increases through T_g. Fig. 2b shows that experimental values of modulus above T_g are not zero-valued, but are 2–3 orders of magnitude smaller than the values below T_g. Thus, eqn (6) is only an approximation for temperatures above T_g, but is sufficiently accurate for the purposes of predicting the

relative elastic response of the polymer over the entire temperature range.

Close examination of Fig. 3b shows that the curves do not exactly exhibit a sigmoidal shape, that is, for higher values of τ beyond the center of the sigmoid, the storage modulus continues to increase by a steady amount (modulus is a function of temperature in the glassy regime). Therefore, the τ^* multiplier in eqn (6) is used to correct the sigmoid for this discrepancy. From Fig. 3b it is also evident that the maximum value of the modulus for each degree of cure proxy follows the same trend observed in Fig. 2c, that is, the maximum value is the greatest for $\phi = 65\%$. Once again, the maximum value of the modulus would be expected to occur at $\phi = 100\%$ if these curves were from epoxies with intermediate degrees of cure, instead of proxies. However, as explained above, the proxy systems were used to characterize eqn (5)–(8) because of the convenience of obtaining modulus data for a range of degrees of cure and temperature using proxy systems. The values for τ_*^a and τ_*^b were determined by quantifying the discrepancy between the modulus values from the DMA data just above the sigmoidal jump and the modulus of the full stoichiometry system at room temperature. The relationship between these discrepancy values and their corresponding τ values were fit with the power law relationship of eqn (8). The corresponding phenomenological parameters are $\tau_*^a = 0.065$ and $\tau_*^b = 0.065$.

Finally, with the initial guess values of eight out of nine phenomenological parameters determined, the final parameter, τ_σ, which describes the relative steepness of the sigmoid jumps shown in Fig. 3b, was determined using a least-squares fit of eqn (3)–(8) to the DMA data shown in Fig. 3b, with a value of $\tau_\sigma = 0.009$. The values of the initial guesses are summarized in Table 2.

5.2 Optimization of parameters

After the initial guesses of all the parameters were determined, they were used in the Newton–Raphson iterative optimization technique to determine the final optimized values of the full set of nine parameters. The optimized values are provided in Table 2. Fig. 3b shows the storage modulus calculated with eqn (3)–(8) and the optimized values plotted against the τ

Table 2 Material parameters for the viscous mapping (all values are dimensionless)

Phenomenological material parameter	Optimized values
α_a	0.0147
α_b	1.0849
ϕ_0	0.4412
ϕ_σ	0.0240
τ_0^a	−0.5097
τ_0^b	0.5537
τ_*^a	0.0778
τ_*^b	0.0424
τ_σ	0.0098

parameter. It is important to note that the model predicts the room temperature modulus of each system to be equal to that of the full stoichiometry system. The model parameters were fit this way to offset the effect of using a series of proxy systems instead of fully stoichiometric systems at partial degrees of cure.

6. Application of mapping to MD predictions

It is uncommon for all the crosslinking reactions that can occur in a thermoset network to actually occur because of steric hindrance constrains on the motion of the reactive groups.[48,49] The degree of cure is defined as the relative amount of conversion that has occurred in a thermosetting polymer system, ranging from 0 (no crosslinking reactions have occurred) to 1.0 (100% of all crosslinking reactions have occurred that can possibly occur given steric hindrance constraints). Conversely, the crosslink density, as defined above, indicates the relative number of crosslinking reactions that have occurred with respect to the total number of reactive group pairs that exist in the material. Therefore, it is typical for a crosslink density to never reach 100%, but a degree of cure can always reach 100% given a sufficiently long cure time. Because the crosslink density is a convenient metric to track with MD, but degree of cure is more convenient from a processing perspective, it is necessary to convert the crosslink densities simulated with MD to degree of cure quantified experimentally. With these definitions, the degree of cure can be determined from the crosslink density as follows:

- The degree of cure is 0 when the crosslink density is 0
- The degree of cure is 1 when the crosslink density has reached its maximum value for a given material
- Intermediate values of the degree of cure are calculated using a linear scaling such that the degree of cure is the ratio of the crosslink density to the maximum crosslink density

MD simulations were reported by Patil et al.[38] to predict the Young's modulus of the same DGEBF/DETDA epoxy system studied herein as a function of crosslinking density. In this study, after converting the data of Patil et al. to be a function of degree of cure, the mapping functions from eqn (3)–(8) were applied using the optimized parameters shown in Table 2. It is emphasized that the MD data of Patil et al. was not used to parameterize the mapping function, it was simply used for

mapping to the corrected state given the strain rate, temperature, and degree of cure effects.

The viscous response of thermoset materials is only apparent in deformations with a finite deviatoric (shape changing) component of deformation. For hydrostatic (volume changing) deformations, the response is purely elastic.[50] Therefore, it is possible to predict the viscous response of the Poisson's ratio (ν) for the isotropic epoxy system as a function of degree of cure, temperature, and strain rate through the standard elasticity equation

$$\nu = \frac{3K - E}{6K} \qquad (9)$$

where K is the bulk modulus, which was predicted by Patil et al.[38] for this epoxy system as a function of crosslink density. Thus, the Poisson's ratio was determined for a range of degrees of cure at room temperature.

7. Results

Fig. 4a shows the mapped MD-predicted Young's modulus for varying temperatures (solid lines) compared with the room temperature raw MD Young's modulus predictions (open circles) with a linear regression fit (dashed line). The experimental data points are included (open diamonds) at varying temperatures, as well as a data point from Littell et al.[45] at 80 °C. As expected, the predicted and measured Young's moduli decrease with increasing temperatures and decreasing degrees of cure. At increasing temperatures, intermolecular distances increase because of increasing thermal fluctuations. As a consequence, there is a decrease in intermolecular forces and a corresponding decrease in the Young's modulus. At lower degrees of cure, the epoxy network is sparsely connected, thus there are fewer covalent bonds between the monomers. Thus, the network is unable to sustain any significant load, manifesting in a lower Young's modulus.

The mapped modulus for the fully crosslinked state ($\phi = 1$) at all temperatures agrees well with the experimental data, although the mapping is less accurate for room temperature relative to temperatures of 80 °C and above. The reason that the mapping at 27 °C and $\phi = 1$ slightly underpredicts the experimental value involves the disagreement of the experimental data between the experiments described herein and those described by Littell et al.[45] The room temperature storage modulus from Fig. 2 is about 2.4 GPa, while the value reported by Littell et al. is about 2.7 GPa. Because the parameterization was performed with the data in Fig. 2 and not with the data from Littell et al., the difference of 0.3 GPa between the two values is apparent in Fig. 4a.

The mapped modulus at 80 °C at degrees of cure above the gel point of the DGEBF/DETDA system ($\phi = 0.6$)[38] is slightly higher than the experimental value before it reduces to match the experimental value as the model approaches the fully crosslinked state. This discrepancy, as explained above, is due to the use of proxy materials systems as a substitute for the full stoichiometry epoxy system with intermediate degrees of cure.
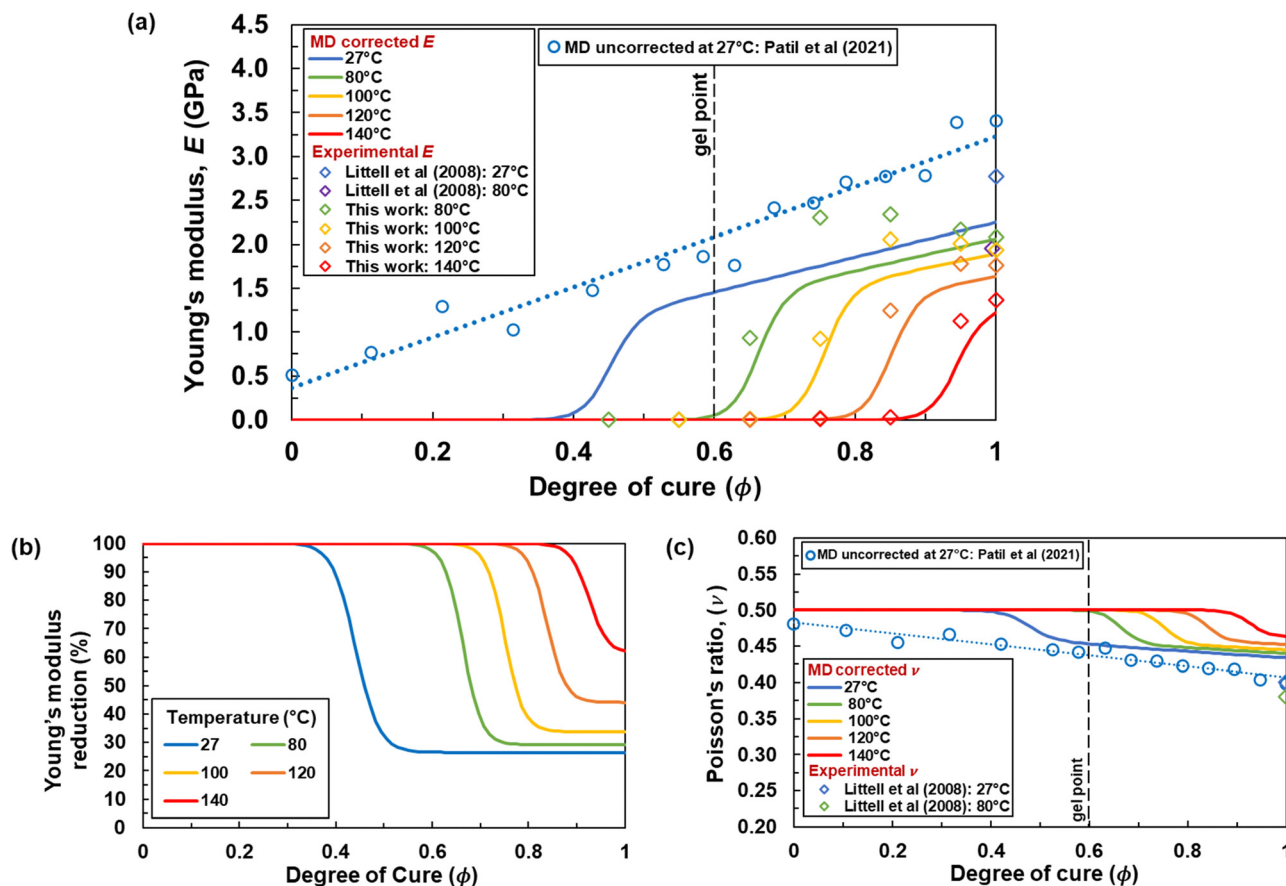
Fig. 4 (a) Plot of raw MD (open circles) and mapped (solid lines) Young's modulus vs. degree of cure for varying temperatures along with experimental data (open diamonds), (b) plot of mapped Young's modulus reduction vs. degree of cure for varying temperatures, (c) plot of raw MD (open circles) and mapped (solid lines) Poisson's ratio vs. degree of cure for varying temperatures along with experimental data (open diamonds).

As the temperature increases, the mapped moduli exhibit improved agreement with the experimental data both below and above gel point. Also, as the temperature approaches 140 °C, the modulus approaches a near zero value as the material advances toward the transition from glassy to rubbery states (shown in Fig. 2c, 155 °C). At 177 °C (the processing temperature for this epoxy system), the modulus is expected to reduce to zero because the material is in the rubbery state and unable to sustain any appreciable mechanical load. This behavior is similar to that observed in Fig. 2a, where the storage modulus goes to zero at 177 °C.

Perhaps the most striking feature of Fig. 4a is the overall significance of the viscous mapping on the MD predicted modulus values. Fig. 4b shows the overall reduction in the MD predicted modulus as a function of degree of cure and temperature. It can be seen that the mapping reduction is highest for low degrees of cure and high temperatures, and lowest for high degrees of cure and low temperatures. Thus, the need for the mapping in MD predictions of thermoset properties is clearly evident for not only strain rates, but for temperatures and degrees of cure as well. Mapped mechanical properties of thermoset and thermoplastic materials can then be used in a process modeling framework to predict and optimize

the processing and properties of composite laminates and structures.[15,22,51–61]

Fig. 4c shows the mapped MD-predicted Poisson's ratio for varying temperatures (solid lines) compared with the room temperature raw MD predicted Poisson's ratio predictions (open blue circles) with a linear regression fit (dashed line). An experimental data point from Littell et al.[45] at 80 °C is also included (open diamond). The predicted Poisson's ratio increases with increasing temperatures, in agreement with experiment,[62–67] because of increased molecular motion. The predicted Poisson's ratio generally decreases with increasing degrees of cure, as observed experimentally.[68,69] Similar to the discussion above regarding the discrepancy between the mapped MD values and the experimental results of Littell et al.,[45] it is important to note that the mapping was parameterized with the experimental data obtained herein, and not the data from Littell et al. The corresponding discrepancy in the experimental results leads to the apparent differences between the experimental and predicted Poisson's ratios at $\phi = 1$.

In the fully cured state ($\phi = 1$), the predicted Poisson's ratios show no significant difference with respect to temperature. Littell et al.[45] also observed an insignificant difference in the experimentally measured Poisson's ratio of 0.4, 0.4 and 0.38 at

temperatures of 27 °C, 50 °C and 80 °C, respectively, from tensile tests at a strain rate of 1×10^{-1} s^{-1}.

As the temperature approaches 140 °C (near the T_g, as shown in Fig. 2c), the mapped MD Poisson's ratio approaches an asymptotic value of 0.5, similar to an incompressible liquid. For 177 °C (above the T_g), the Poisson's ratio is expected to reach 0.5 for the entire range of degree of cure. This behavior of the MD-mapped Poisson's ratio with temperature agrees well with experimental observations.[65–69]

8. Conclusions

An efficient phenomenological-based mapping function has been developed for correlating raw MD-predicted elastic properties of thermosets that exhibit significant viscoelastic effects, such as the DGEBF/DETDA epoxy system studied herein, to the corresponding time-dependent laboratory-based properties. This approach satisfies the three requirements articulated at the beginning of this study. First, the method requires only minimal MD simulations. Only MD predictions of the mechanical properties of the polymer at multiple degrees of cure are needed, as opposed to an ambitious program of simulations to establish the time-temperature superposition relationship. Second, the method requires minimal experimental input. Only the storage modulus from DMA temperature sweep tests on off-stoichiometry specimens are required, and not the rigorous experimental characterization of the full viscoelastic constitutive response. Third, this approach directly addresses the well-known major issues associated with the inability of all-atom MD to fully simulate conformational relaxation processes at nanosecond timescales. Specifically, the over-estimation of mechanical properties at MD-scale strain rates, at temperatures above T_g, and at intermediate degrees of cure.

It's important to note that this approach is intended for efficient mapping of MD-predicted properties of viscoelastic thermosets. This level of efficiency is particularly beneficial for materials engineering environments where computational material design and process optimization need to be performed in a timely manner. This approach is not a direct substitute for comprehensive characterization of viscoelastic constitutive models or complete quantification of properties at intermediate degrees of cure. However, it does offer a simple approach to map MD simulation data for the strain-rate effect and the overestimation of properties at elevated temperatures and intermediate degrees of cure.

Although the proposed approach does require experimental input (strain-rate dependence on elastic response and DMA temperature sweep data), the effort and resources required to obtain this input is far less than that required to obtain fully-characterized time-temperature superposition data. This approach only requires some basic characterization of the viscous response of the polymer. Thus, this approach provides a means to efficiently establish a mapping function for transforming raw MD data into MD data that can be immediately used for further multi-scale analysis.

Author contributions

SUP: conceptualization, data curation, investigation, methodology, visualization, writing – original draft, writing – review & editing; ASK: investigation, formal analysis; LKO: investigation; UY: investigation; JAK: project administration; MM: funding acquisition, project administration, writing – review & editing; GMO: conceptualization, data curation, formal analysis, funding acquisition, investigation, methodology, project administration, resources, supervision, writing – original draft, writing – review & editing.

Data availability

The raw/processed data required to reproduce these findings cannot be shared at this time as the data also forms part of an ongoing study.

Conflicts of interest

There are no conflicts to declare.

Acknowledgements

References

1 G. M. Odegard and A. Bandyopadhyay, Physical aging of epoxy polymers and their composites, *J. Polym. Sci., Part B: Polym. Phys.*, 2011, **49**(24), 1695–1716.

2 C. E. Estridge, The effects of competitive primary and secondary amine reactivity on the structural evolution and properties of an epoxy thermoset resin during cure: a molecular dynamics study, *Polymer*, 2018, **141**, 12–20.

3 S. V. Kallivokas, A. P. Sgouros and D. N. Theodorou, Molecular dynamics simulations of EPON-862/DETDA epoxy networks: structure, topology, elastic constants, and local dynamics, *Soft Matter*, 2019, **15**(4), 721–733.

4 C. Li and A. Strachan, Molecular dynamics predictions of thermal and mechanical properties of thermoset polymer EPON862/DETDA, *Polymer*, 2011, **52**(13), 2920–2928.

5 C. Li and A. Strachan, Molecular scale simulations on thermoset polymers: a review, *J. Polym. Sci., Part B: Polym. Phys.*, 2015, **53**(2), 103–122.

6 G. M. Odegard, B. D. Jensen, S. Gowtham, J. Wu, J. He and Z. Zhang, Predicting mechanical response of crosslinked epoxy using ReaxFF, *Chem. Phys. Lett.*, 2014, **591**, 175–178.

7 G. M. Odegard, S. U. Patil, P. P. Deshpande, K. Kanhaiya, J. J. Winetrout, H. Heinz, S. P. Shah and M. Maiaru, Molecular Dynamics Modeling of Epoxy Resins Using the Reactive Interface Force Field, *Macromolecules*, 2021, **54**(21), 9815–9824.

8 M. S. Radue, B. D. Jensen, S. Gowtham, D. R. Klimek-Mcdonald, J. A. King and G. M. Odegard, Comparing the Mechanical Response of Di-, Tri-, and Tetra-functional Resin Epoxies with Reactive Molecular Dynamics, *J. Polym. Sci., Part B: Polym. Phys.*, 2018, **56**(3), 255–264.

9 M. S. Radue, V. Varshney, J. W. Baur, A. K. Roy and G. M. Odegard, Molecular Modeling of Cross-Linked Polymers with Complex Cure Pathways: A Case Study of Bismaleimide Resins, *Macromolecules*, 2018, **51**(5), 1830–1840.

10 T. W. Sirk, K. S. Khare, M. Karim, J. L. Lenhart, J. W. Andzelm, G. B. Mckenna and R. Khare, High strain rate mechanical properties of a cross-linked epoxy across the glass transition, *Polymer*, 2013, **54**(26), 7048–7057.

11 M. Tsige, C. D. Lorenz and M. J. Stevens, Role of Network Connectivity on the Mechanical Properties of Highly Cross-Linked Polymers, *Macromolecules*, 2004, **37**(22), 8466–8472.

12 V. Varshney, S. S. Patnaik, A. K. Roy and B. L. Farmer, A Molecular Dynamics Study of Epoxy-Based Networks: Cross-Linking Procedure and Prediction of Molecular and Material Properties, *Macromolecules*, 2008, **41**(18), 6837–6842.

13 A. Vashisth, C. Ashraf, W. Zhang, C. E. Bakis and A. C. T. Van Duin, Accelerated ReaxFF Simulations for Describing the Reactive Cross-Linking of Polymers, *J. Phys. Chem. A*, 2018, **122**(32), 6633–6642.

14 G. M. Odegard, S. U. Patil, P. S. Gaikwad, P. Deshpande, A. S. Krieg, S. P. Shah, A. Reyes, T. Dickens, J. A. King and M. Maiaru, Accurate predictions of thermoset resin glass transition temperatures from all-atom molecular dynamics simulation, *Soft Matter*, 2022, **18**(39), 7550–7558.

15 S. U. Patil, S. P. Shah, M. Olaya, P. P. Deshpande, M. Maiaru and G. M. Odegard, Reactive Molecular Dynamics Simulation of Epoxy for the Full Cross-Linking Process, *ACS Appl. Polym. Mater.*, 2021, **3**(11), 5788–5797.

16 H. Al Mahmud, S. U. Patil, M. S. Radue and G. M. Odegard, Probing the Influence of Surface Chemical Functionalization on Graphene Nanoplatelets-Epoxy Interfacial Shear Strength Using Molecular Dynamics, *Nanomaterials*, 2023, **13**(2), 287.

17 A. Aramoon, T. D. Breitzman, C. Woodward and J. A. El-Awady, Coarse-Grained Molecular Dynamics Study of the Curing and Properties of Highly Cross-Linked Epoxy Polymers, *J. Phys. Chem. B*, 2016, **120**(35), 9495–9505.

18 S. Yang, Z. Cui and J. Qu, A Coarse-Grained Model for Epoxy Molding Compound, *J. Phys. Chem. B*, 2014, **118**(6), 1660–1669.

19 M. Langeloth, T. Sugii, M. C. Böhm and F. Müller-Plathe, The glass transition in cured epoxy thermosets: a comparative molecular dynamics study in coarse-grained and atomistic resolution, *J. Chem. Phys.*, 2015, **143**(24), 243158.

20 C. Li and A. Strachan, Coarse-grained molecular dynamics modeling of reaction-induced phase separation, *Polymer*, 2018, **149**, 30–38.

21 S. Yang and J. Qu, Coarse-grained molecular dynamics simulations of the tensile behavior of a thermosetting polymer, *Phys. Rev. E: Stat., Nonlinear, Soft Matter Phys.*, 2014, **90**(1), 012601.

22 S. P. Shah, S. U. Patil, C. J. Hansen, G. M. Odegard and M. Maiarù, Process modeling and characterization of thermoset composites for residual stress prediction, *Mech. Adv. Mater. Struct.*, 2023, **30**(3), 486–497.

23 O. G. Kravchenko, C. Li, A. Strachan, S. G. Kravchenko and R. B. Pipes, Prediction of the chemical and thermal shrinkage in a thermoset polymer, *Composites, Part A*, 2014, **66**, 35–43.

24 H. Park, J. Choi, B. Kim, S. Yang, H. Shin and M. Cho, Toward the constitutive modeling of epoxy matrix: temperature-accelerated quasi-static molecular simulations consistent with the experimental test, *Composites, Part B*, 2018, **142**, 131–141.

25 H. Park and M. Cho, A multiscale framework for the elasto-plastic constitutive equations of crosslinked epoxy polymers considering the effects of temperature, strain rate, hydrostatic pressure, and crosslinking density, *J. Mech. Phys. Solids*, 2020, **142**, 103962.

26 C. Park, J. Jung and G. J. Yun, Multiscale micromorphic theory compatible with MD simulations in both time-scale and length-scale, *Int. J. Plast.*, 2020, **129**, 102680.

27 C. Park, J. Jung, T. Park and G. Yun, Multiscale Micromorphic Theory and Simulation with Co-existing Molecular and Continuum Time Scales, in *AIAA Scitech 2020 Forum*.

28 K. S. Khare and F. R. Phelan Jr., Integration of Atomistic Simulation with Experiment Using Time–Temperature Superposition for a Cross-Linked Epoxy Network, *Macromol. Theory Simul.*, 2020, **29**(2), 1900032.

29 K. S. Khare and F. R. Phelan, Quantitative Comparison of Atomistic Simulations with Experiment for a Cross-Linked Epoxy: A Specific Volume–Cooling Rate Analysis, *Macromolecules*, 2018, **51**(2), 564–575.

30 A. J. Levine and S. T. Milner, Star Polymers and the Failure of Time–Temperature Superposition, *Macromolecules*, 1998, **31**(24), 8623–8637.

31 J. Zou, F. You, L. Su, Z. Yang, G. Chen and S. Guo, Failure mechanism of time-temperature superposition for poly(vinyl chloride)/dioctylphthalate (100/70) system, *J. Appl. Polym. Sci.*, 2012, **124**(1), 452–458.

32 M. N. Olaya, G. M. Odegard and M. Maiaru, A Novel Approach to Characterization of Composite Polymer Matrix Materials for Integrated Computational Materials Engineering Approaches, in *AIAA Scitech 2021 Forum*.

33 M. N. Olaya, S. S. Shah and M. Maiaru, Thermoset Polymers Characterization as a Function of Cure State Using Off-Stoichiometry Proxies, *ChemRxiv*, 2022, preprint, DOI: **10.26434/chemrxiv-2022-ddlc9**.

34 R. M. Christensen, *Theory of Viscoelasticity An Introduction*, Academic Press, 2nd edn, 1982.

35 W. N. Findley, J. S. Lai and K. Onaran, *Creep and Relaxation of Nonlinear Viscoelastic Materials*, Dover Publications, 2011.

36 E. Buckingham, On Physically Similar Systems; Illustrations of the Use of Dimensional Equations, *Phys. Rev.*, 1914, **4**(4), 345–376.

37 J. J. Winetrout, K. Kanhaiya, G. Sachdeva, R. Pandey, B. Damirchi, D. Adri Van, G. M. Odegard and H. Heinz, *Implementing Reactivity in Molecular Dynamics Simulations with the Interface Force Field (IFF-R) and Other Harmonic Force Fields*, arXiv, 2021, preprint, arXiv.2107.14418, DOI: **10.48550/arXiv.2107.14418**.

38 S. U. Patil, S. P. Shah, M. Olaya, P. P. Deshpande, M. Maiaru and G. M. Odegard, Reactive Molecular Dynamics Simulation of Epoxy for the Full Cross-Linking Process, *ACS Appl. Polym. Mater.*, 2021, **3**(11), 5788–5797.

39 W. A. Pisani, M. S. Radue, S. Chinkanjanarot, B. A. Bednarcyk, E. J. Pineda, K. Waters, R. Pandey, J. A. King and G. M. Odegard, Multiscale modeling of PEEK using reactive molecular dynamics modeling and micromechanics, *Polymer*, 2019, **163**, 96.

40 L. Pauling, E. Bright and J. Wilson, *Introduction to Quantum Mechanics: with Applications to Chemistry*, Dover Publications, 1985.

41 A. Rahman, P. Deshpande, M. S. Radue, G. M. Odegard, S. Gowtham, S. Ghosh and A. D. Spear, A machine learning framework for predicting the shear strength of carbon nanotube-polymer interfaces based on molecular dynamics simulation data, *Compos. Sci. Technol.*, 2021, **207**, 108627.

42 G. M. Odegard, T. S. Gates and H. M. Herring, Characterization of viscoelastic properties of polymeric materials through nanoindentation, *Exp. Mech.*, 2005, **45**(2), 130–136.

43 A. Galántai, The theory of Newton's method, *J. Comput. Appl. Math.*, 2000, **124**(1), 25–44.

44 D. R. Klimek-Mcdonald, J. A. King, I. Miskioglu, E. J. Pineda and G. M. Odegard, Determination and Modeling of Mechanical Properties for Graphene Nanoplatelet/Epoxy Composites, *Polym. Compos.*, 2018, **39**(6), 1845–1851.

45 J. D. Littell, C. R. Ruggeri, R. K. Goldberg, G. D. Roberts, W. A. Arnold and W. K. Binienda, Measurement of Epoxy Resin Tension, Compression, and Shear Stress-Strain Curves over a Wide Range of Strain Rates Using Small Test Specimens, *J. Aerosp. Eng.*, 2008, **21**(3), 162–173.

46 A. Gilat, R. K. Goldberg and G. D. Roberts, Strain Rate Sensitivity of Epoxy Resin in Tensile and Shear Loading, *J. Aerosp. Eng.*, 2007, **20**(2), 75–89.

47 D. S. Sholl and J. A. Steckel, *Density Functional Theory A Practicle Introduction*, John Wiley & Sons, Inc., 2009.

48 M. S. Radue, B. D. Jensen, S. Gowtham, D. R. Klimek-Mcdonald, J. A. King and G. M. Odegard, Comparing the mechanical response of di-, tri-, and tetra-functional resin epoxies with reactive molecular dynamics, *J. Polym. Sci., Part B: Polym. Phys.*, 2018, **56**(3), 255–264.

49 C. M. Hadden, D. R. Klimek-Mcdonald, E. J. Pineda, J. A. King, A. M. Reichanadter, I. Miskioglu, S. Gowtham and G. M. Odegard, Mechanical properties of graphene nanoplatelet/carbon fiber/epoxy hybrid composites: multiscale modeling and experiments, *Carbon*, 2015, **95**, 100–112.

50 P. J. Flory, *Principles of polymer chemistry*, Cornell University Press, Ithaca, 1953.

51 S. U. Patil, S. S. Shah, P. P. Deshpande, K. Kashmari, G. M. Odegard and M. Maiaru, Prediction Of Residual Stress Build-Up In Polymer Matrix Composite During Cure Using A Two-Scale Approach in Proceedings of the American Society for Composites—Thirty-fourth Technical Conference, 2019.

52 S. U. Patil, S. S. Shah, P. P. Deshpande, K. Kashmari, M. N. Olaya, G. M. Odegard and M. Maiaru, Multi-scale Approach to Predict Cure-Induced Residual Stresses in an Epoxy System in Proceedings of the American Society for Composites—Thirty-fifth Technical Conference, 2020.

53 P. P. Deshpande, S. S. Shah, S. U. Patil, K. Kashmari, M. N. Olaya, G. M. Odegard and M. Maiaru, Multiscale Modelling of the Cure Process in Thermoset Polymers using ICME in Proceedings of the American Society for Composites—Thirty-fifth Technical Conference, 2020.

54 P. P. Deshpande, S. S. Shah, S. U. Patil, K. Kashmari, G. M. Odegard and M. Maiaru A Multi-Scale Approach For Modelling The Cure Of Thermoset Polymers Within ICME in Proceedings of the American Society for Composites—Thirty-fourth Technical Conference, 2019.

55 S. S. Shah, S. U. Patil, P. P. Deshpande, K. Kashmari, G. M. Odegard and M. Maiaru, Multiscale modeling of thermoset composite to predict process-induced residual stresses, in ICCM22, Engineers Australia, 2019.

56 S. P. Shah and M. Maiarù, Effect of Manufacturing on the Transverse Response of Polymer Matrix Composites, *Polymers*, 2021, **13**(15), 2491.

57 M. Maiaru, Effect of uncertainty in matrix fracture properties on the transverse strength of fiber reinforced polymer matrix composites, in 2018 AIAA/ASCE/AHS/ASC Structures, Structural Dynamics, and Materials Conference.

58 R. J. D'mello, A. M. Waas, M. Maiaru and R. Koon, Integrated Computational Modeling for Efficient Material and Process Design for Composite Aerospace Structures, in AIAA Scitech 2020 Forum.

59 S. Shah, S. Patil, P. Deshpande, A. Krieg, K. Kashmari, H. A. Mahmud, J. King, G. M. Odegard and M. Maiaru, Multiscale Modeling for Virtual Manufacturing of Thermoset Composites, in AIAA Scitech 2020 Forum.

60 P. S. Gaikwad, A. S. Krieg, P. P. Deshpande, S. U. Patil, J. A. King, M. Maiaru and G. M. Odegard, Understanding the Origin of the Low Cure Shrinkage of Polybenzoxazine Resin by Computational Simulation, *ACS Appl. Polym. Mater.*, 2021, **3**(12), 6407–6415.

61 S. S. Shah and M. Maiaru, Microscale analysis of virtually cured polymer matrix composites accounting for uncertainty in matrix properties during manufacturing, in Proceedings of the American Society for Composites-Thirty-third Technical Conference, Seattle, USA, 2018.

62 V. H. Carneiro and H. Puga, Temperature Variability of Poisson's Ratio and Its Influence on the Complex Modulus Determined by Dynamic Mechanical Analysis, *Technologies*, 2018, **6**(3), 81.

63 S. Pandini and A. Pegoretti, Time, temperature, and strain effects on viscoelastic Poisson's ratio of epoxy resins, *Polym. Eng. Sci.*, 2008, **48**(7), 1434–1441.

64 C. M. Migwi, M. I. Darby, G. H. Wostenholm, B. Yates, M. Moss and R. Duffy, A method of determining the shear

modulus and Poisson's ratio of polymer materials, *J. Mater. Sci.*, 1994, **29**(13), 3430–3432.

65 P. H. Mott, J. R. Dorgan and C. M. Roland, The bulk modulus and Poisson's ratio of ''incompressible'' materials, *J. Sound Vib.*, 2008, **312**(4), 572–575.

66 A. Tcharkhtchi, S. Faivre, L. E. Roy, J. P. Trotignon and J. Verdu, Mechanical properties of thermosets, *J. Mater. Sci.*, 1996, **31**(10), 2687–2692.

67 L. Yang, L. Yang and R. L. Lowe, A viscoelasticity model for polymers: time, temperature, and hydrostatic pressure dependent Young's modulus and Poisson's ratio across transition temperatures and pressures, *Mech. Mater.*, 2021, **157**, 103839.

68 D. J. O'brien, N. R. Sottos and S. R. White, Cure-dependent Viscoelastic Poisson's Ratio of Epoxy, *Exp. Mech.*, 2007, **47**(2), 237–249.

69 S. Saseendran, M. Wysocki and J. Varna, Cure-state dependent viscoelastic Poisson's ratio of LY5052 epoxy resin, *Adv. Manuf.: Polym. Composites Sci.*, 2017, **3**(3), 92–100.